

## Short Paper

---

# Analysis and Comparison of Various Shape Mirrors Used in Omnidirectional Cameras with Parameter Variation\*

KUO-YANG TU

*Institute of System Information and Control  
National Kaohsiung First University of Science and Technology  
Kaohsiung, 811 Taiwan*

The studies on omnidirectional cameras usually focus on design and/or development of the complicated structure for a wide range of view. However, difficult calibration and expensive cost arisen from the complicated structure of omnidirectional cameras are considerable. In this paper, imprecise parameters resulted from missing calibration of the reflective mirrors of various profiles in omnidirectional cameras are studied. The relationship between an object surface and an image plane, related to camera parameters, is thus derived. In addition, an algorithm of more perfect unwarped images in omnidirectional cameras is proposed. In practical, it is difficult and costly to make an omnidirectional camera consisted of the reflective mirrors of various profiles. Therefore, a simulator based on the derived relationship is designed to compare the omnidirectional camera of various profile mirrors influenced by parameter variations. There are five kinds of reflective mirrors with distinct profiles, spherical, parabolic, conical, tangent and sine, respectively, compared in same size. In addition, the profile to compare the variation of these five mirrors is included.

**Keywords:** catadioptric sensors, parameter calibration, mirror profiles, unwarped images, image processing

## 1. INTRODUCTION

The studies on omnidirectional (360 degrees) cameras usually focus on the design and/or development of the complicated structure for a wide range of view. The omnidirectional field of view could be applied in a variety of realms such as autonomous navigation, videoconference, virtual reality and remote monitoring. Over the past 15 years, researchers have studied a number of papers concerned with omnidirectional cameras and their application. The studies for a wide range of view make innovative features developed in consumer cameras possible for the future. Research about omnidirectional cameras becomes popular in the last decade.

The complicated structure of omnidirectional cameras can be distinguished by two types: use of special lenses and use of convex mirrors [1]. There are two kinds of special lenses: fish-eye lenses and panoramic annular lenses. Using fish-eye lenses, Morita proposed a motion stereo algorithm for measuring the three dimensional lines by moving a

---

Received June 27, 2007; revised April 2 & June 16 & August 26, 2008; accepted September 11, 2008.

Communicated by Pau-Choo Chung.

\* This paper was partially supported by the National Science Council of Taiwan, R.O.C. under grants No. NSC 94-2213-E-327-014-.

single camera linearly and processing the grabbed sequential multiple images [2]. Researchers at the University of Cincinnati applied a fish-eye camera to position control of mobile robots [3, 4]. Fish-eye lenses are a good commercial optics for wide view, but unsuitable for computer vision because without a single view point the images are distorted. Therefore, Greguss proposed a Panoramic Annular Lens (PAL) to acquire a distortion free panoramic image [5, 6]. The complicated structure of PAL makes it difficult to increase the view field of tilt angles.

There are four kinds of convex mirrors used in omnidirectional cameras: conical, spherical, hyperboloidal and paraboloidal mirrors. The image captured via a conical mirror has severe warp in center regions, but good resolution in rim regions. Yagi developed the omnidirectional image sensors, named COPIS, together with an image processing method for robot navigation [7, 8]. Like the fish-eye lens, an image captured by a spherical mirror has rather good resolution in the center region but poor resolution in the rim regions. A spherical mirror assists to catch all images around it, and the field of its view is the widest among sensors with convex mirrors [9, 10]. However, the single center projection is not satisfied in the geometrical relation. The hyperboloidal mirror possesses a focal point, which easily generates any desired image projected on any designated image plane, such as a perspective image or a panoramic image, from an omnidirectional input. Yamazawa et al. proposed an omnidirectional image sensor using a hyperboloidal mirror named HyperOmni Vision [11, 12]. The lower angle of HyperOmni Vision like that of a spherical mirror has good resolution, so does the upper angle of HyperOmni Vision like that of a conical mirror. In a word, HyperOmni Vision has the advantage of both spherical and conical mirrors. A paraboloidal mirror proposed by Peri and Nayar [13, 14] is another optic usage which has a single center of projection. The view field of the paraboloidal mirror and the resolution of the omnidirectional image are just between the hyperboloidal mirror and the spherical mirror.

Omnidirectional cameras are complicated due to parameter variations, and expensive for precise design and manufacturing. Both block the studies of omnidirectional cameras influenced by parameter variations. In this paper, the characteristics of various profile mirrors used for omnidirectional cameras are analyzed for studying the influence of parameter variations. To investigate the influence of omnidirectional camera performance due to missing precise calibration, a new approximation relationship between object surfaces and image planes is derived. After that, the derived relationship changed with respect to the parameter variation reveals the performance of the omnidirectional camera influenced by the mirrors of distinct profiles.

In addition to spherical, parabolic, and conical mirrors, the study on two new types of mirrors, tangent and sine mirrors, are included. Many researches consider that a single viewpoint is the primary design goal of omnidirectional cameras [15]. However, many applications such robot navigation may not be restricted by having a single viewpoint [16]. That is because the image processed for robot is unlike for human who needs clear picture. Therefore, the author would like to study the innovative kinds of mirrors, sine and tangent shapes.

It, however, is difficult to produce real reflective mirrors for studying the performance of omnidirectional cameras with practical experiments. There are at least two difficulties. First is about cost. A reflective mirror is expensive, so it will be a costly study for distinct reflective mirrors installed in an omnidirectional camera for comparing. Second

is about measurement. Captured image is very sensitive to light conditions, and it is complicated to accurately calculate the geometric relationship between the object surface and an image sensor. These two difficulties block the study of various reflective mirrors used in omnidirectional cameras. In this paper, a simulator for studying various mirrors in omnidirectional cameras is designed and implemented. The study focuses on distinct geometric profiles of catoptric mirrors. Five mirrors whose profiles are spherical, parabolic, conical, tangent and sine are installed in an omnidirectional camera for comparing their characteristics. In particular, mirrors of both tangent and sine which are able to result in distorted images are less revealed in the literature. The image influenced by parameter variation motivates the study of innovative mirror profiles such as tangent and sine. Study results show that both innovative mirror profiles have robust characteristics against parameter variation. In this paper, the study paves a way to develop innovative features for robot vision in the future.

The rest of this paper is organized as follows. In section 2, the basic relationship between an object surface and an image plane, grounded for a new approximation in section 3, is derived. In section 4, the derived relationship implements a simulator summarized by a calculation procedure for researching and developing innovative omnidirectional cameras. The mirror profiles of the omnidirectional camera influenced by parameter variation are studied in section 5. Finally, conclusion and discussions are made in section 6.

## 2. PRELIMINARIES

The studies on omnidirectional cameras usually focus on the linear relationship between an object surface and an image plane [17]. This linear relationship has the benefit that it doesn't need computation to take an original image, but restricts the application realms of omnidirectional cameras. So, Yagi *et al.* designed a conical projection image sensor to extend vision range for robot navigation [8]. Lima *et al.* designed a mirror consisted of three parts, isometric, constant curvature and planar, so that the captured image can cover both far and near range. Stimulated by these researches, it is interesting of the application realms of omnidirectional cameras exploited by designing mirror profiles.

In a study of omnidirectional camera, it is important to solve relationships between object surfaces and image planes via a designated mirror surface. Suppose that a fixed object surface  $S \in \mathbf{R}^3$  captured by catadioptric sensors is given and an image sensor in a camera consists of an image plane  $I \in \mathbf{R}^2$ . A given mirror surface  $M \in \mathbf{R}^3$  achieves a transformation  $T_M$  from some subset of  $I$  to  $S$ . The transformation  $T_M$  borrows a ray from a point  $q \in I$  until it intersects the mirror at a point  $r \in M$ . As shown in Fig. 1, the physical conduct between object surface and image plane is that image sensor  $I$  captures the image of  $S$  via mirror  $M$ . Therefore, the real relationship should be  $G$ , but researchers usually approximate to  $T_M$ .

Lima *et al.* [18] and Hicks and Bajcsy [17] approached  $T_M$  to differential equations. However, these approach equations don't involve the parameters of an omnidirectional camera. It is inconvenient to study the relationship between object surfaces and image planes, influenced by parameter variation. In this paper, the exact relationship,  $G$ , approximated by linear polynomials is derived. For demonstrating its functions, a simulator of omnidirectional cameras for studying the mirrors of various shapes is implemented.

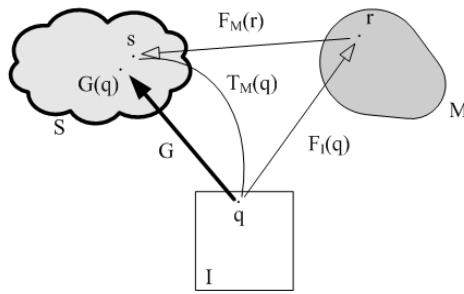


Fig. 1. The calculation scheme of omnidirectional vision systems.

### 3. A NEW APPROXIMATION RELATIONSHIP BETWEEN AN OBJECT SURFACE AND AN IMAGE PLANE

It is intuitive to find the relationship between object surfaces and image planes from an image sensor to an object surface. Because the focal length of a camera is fixed, every pixel in its image sensor maps to a fixed area of mirror surface. By catoptric principle, a given area on a mirror surface maps a fixed scene on an object surface. As shown in Fig. 2, the ray trace  $L_1$  goes through the lens focus from  $(x_r, y_r, z_r) \in M$  on the mirror surface to a point  $(x_q, y_q) \in I$  on the image sensor. The ray  $L_1$  is come from  $L_4$ , the ray trace from  $(x_s, y_s) \in S$  on the object surface to  $(x_r, y_r, z_r)$ . Instead of  $T_M(q)$  proposed in literature [17, 18],  $G$  is approximated by linear Eqs.  $L_1$  and  $L_4$  in this paper. The linear Eqs., as show in Fig. 1, are functions  $F_I(q): I \rightarrow M$ , and  $F_M(r): M \rightarrow S$  as follows

$$r = F_I(q) \tag{1}$$

$$s = F_M(r) \tag{2}$$

where  $q \in I$ ,  $r \in M$ , and  $s \in S$  are the points on the image sensor, mirror surface, and object surface, respectively.

It should note that by optic principle an omnidirectional camera, however, captures an image along the ray from object surface  $S$  to image plane  $I$  that is different from the above mentioned. But, it is difficult to solve a point  $(x_s, y_s) \in S$  shot by  $L_4$  at  $(x_r, y_r, z_r) \in M$  and then along  $L_1$  to reach a pixel cell  $(x_q, y_q) \in I$ . Hence,  $G$  is usually approximated by a relationship from  $I$  to  $S$ .

The relationship from the image plane to the object surface is derived by finding  $L_1$  and  $L_4$  from  $x_q$  to  $x_s$  as shown in Fig. 3. For the sake of simplicity, the following derivation neglects variable  $y$ . Let  $\alpha$  be the angle between  $L_1$  and the image plane. Then, the angle between  $L_1$  and  $V_1$  is  $\frac{\pi}{2} - \alpha$ . Let  $\theta$  be  $\tan^{-1}(\partial z/\partial x)$  (i.e. the curvature of mirror surface). Then the angle between  $V_1$  and  $L_4$  is  $\frac{\pi}{2} - \alpha + 2\theta$ . Therefore, the straight lines  $L_1$  and  $L_4$  are

$$L_1: z = \frac{\lambda}{x_q} x + H, \tag{3}$$

$$L_4 : z(x_{s1}) - z = \frac{x - x_{s1}}{\tan\left(\frac{\pi}{2} - \alpha + 2\theta\right)}, \quad (4)$$

where  $x, z \in \mathbf{M}$ ,  $x_q \in \mathbf{I}$ , and  $x_{s1} \in \mathbf{S}$ . We can obtain the relationship from  $\mathbf{I}$  to  $\mathbf{S}$  by the following Lemma.

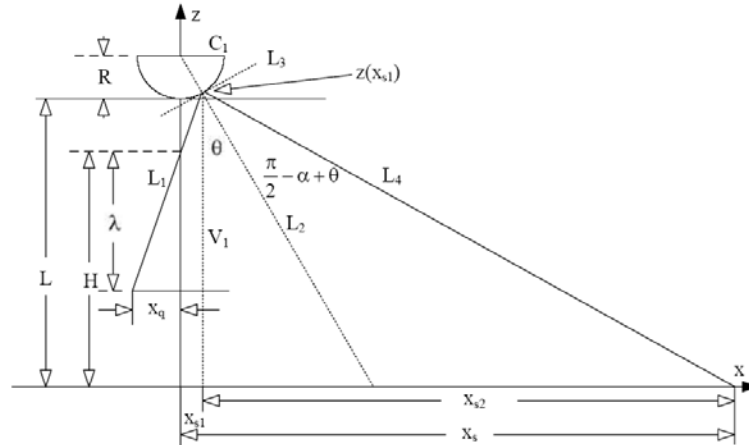


Fig. 2. The relationship between the object surface and the image plane.

**Lemma 1** By a catadioptric sensor as shown in Fig. 2, a point  $x_q$  on the image plane and a point  $x_s$  on the object surface obey the following relationship

$$x_s = \frac{x_q}{\lambda} (z(x_{s1}) - H) + z(x_{s1}) \frac{\frac{x_q}{\lambda} + \frac{2z'(x_r)}{1 - z'(x_r)}}{1 - \frac{x_q}{\lambda} \frac{2z'(x_r)}{1 - z'(x_r)}} \quad (5)$$

where  $x_r \in \mathbf{M}$ ,  $z'(x_r) = \partial z(x_r) / \partial x_r$  is the curvature of the mirror surface,  $\lambda$  is focal length, and  $H$  is camera height from the ground as shown in Fig. 2.

**Proof:** On the object surface, one point satisfies

$$x_s = x_{s1} + x_{s2}. \quad (6)$$

$x_{s1}$  and  $x_{s2}$  can be obtained by solving  $L_1$  and  $L_4$ , respectively. Since  $L_1$  reaches the mirror surface at  $(x_{s1}, z(x_{s1}))$ , Eq. (3) can be rewritten as

$$x_{s1} = \frac{x_q}{\lambda} (z(x_{s1}) - H). \quad (7)$$

Besides, since  $L_4$  reaches the object surface at  $(x_s, 0)$ , manipulating Eq. (4) obtains

$$x_s - x_{s1} = z(x_{s1}) \tan\left(\frac{\pi}{2} - \alpha + 2\theta\right). \quad (8)$$

After manipulating Eq. (6), substituting it into Eq. (8) obtains

$$x_{s2} = z(x_{s1}) \tan\left(\frac{\pi}{2} - \alpha + 2\theta\right). \quad (9)$$

Substituting Eqs. (7) and (9) into Eq. (6) obtains

$$x_s = \frac{x_q}{\lambda} (z(x_{s1}) - H) + z(x_{s1}) \tan\left(\frac{\pi}{2} - \alpha + 2\theta\right). \quad (10)$$

Because

$$\begin{aligned} \tan\left(\frac{\pi}{2} - \alpha\right) &= \frac{x_q}{\lambda}, \text{ and} \\ \tan(\theta) &= z'(x_r) = z'(x_{s1}) \end{aligned}$$

Eq. (10) can be rewritten as

$$x_s = \frac{x_q}{\lambda} (z(x_{s1}) - H) + z(x_{s1}) \frac{\frac{x_q}{\lambda} + \frac{2z'(x_r)}{1 - z'(x_r)}}{1 - \frac{x_q}{\lambda} \frac{2z'(x_r)}{1 - z'(x_r)}} \quad \square$$

Note that Eq. (5) is also expressed by

$$x_s = \frac{x_q}{\lambda} (z(x_r) - H) + z(x_r) \frac{\frac{x_q}{\lambda} + \frac{2z'(x_r)}{1 - z'(x_r)}}{1 - \frac{x_q}{\lambda} \frac{2z'(x_r)}{1 - z'(x_r)}}. \quad (11)$$

Because  $x_{s1} = x_r$  due to  $V_1$  on a parallel with  $z$  axis as shown in Fig. 2. Eq. (5) is more meaningful in expressing the relationship from the image plane to the object surface, while Eq. (11) is more convenient to calculate this relationship.

The relationship from  $x_q$  to  $x_s$  concerns with  $(x_r, z_r)$  (*i.e.*  $(x_{s1}, z(x_{s1}))$ ), a point on the mirror surface. This point is dependent on the mirror profiles. The point  $(x_r, z_r)$  can be solved by the intersection between  $L_1$  and the mirror surface. The curvature of mirror surface decides  $(x_r, z_r)$  how to point  $(x_s, 0)$  on the object surface from Eq. (11). Therefore, the distinct profiles of mirror surface have distinct characteristics. For studying this property in detail, five kinds of mirrors are defined with the same height and width as follows:

$$M_p: z = R + L - \sqrt{R^2 - x^2} \text{ for } |x| \leq w, \text{ and } z \leq h \text{ (spherical mirror)} \quad (12)$$

$$M_{pa}: z = R + L - \sqrt{R^2 - fx^2} \quad (\text{parabolic mirror}) \quad (13)$$

$$M_c: z = \frac{h}{w}x + L \quad (\text{conical mirror}) \quad (14)$$

$$M_t: z = h \times \tan\left(\frac{\pi}{4w}x\right) + L \quad (\text{tangent mirror}) \quad (15)$$

$$M_s: z = h \times \sin\left(\frac{\pi}{2w}x\right) + L \quad (\text{sine mirror}) \quad (16)$$

where  $R$  is the radius of the spherical mirror,  $f$  is the parameter of the parabolic mirror, and  $L$  is the distance from mirrors to ground,  $(x_r, y_r, z_r) \in \mathbf{M}$ ,  $w$  and  $h$  are the width and height of these five mirrors, respectively. These five mirrors are found based on a spherical mirror that is visible by the image sensor of an omnidirectional camera. After the visible area of the spherical mirror (*i.e.*  $w$  and  $h$ ) is found out, the other four mirrors, conical, tangent and sine mirrors, are built according to the found  $w$  and  $h$ . Based on the omnidirectional camera parameters, mirror height  $L = 710\text{mm}$ , camera height  $H = 440\text{mm}$ , mirror radius  $R = 1,200\text{mm}$ , focal length  $\lambda = 3\text{mm}$ , Fig. 3 shows the profiles of these five mirrors in which the width and height of all mirrors are  $w = 335.7226\text{mm}$  and  $h = 47.9191\text{mm}$ , respectively.

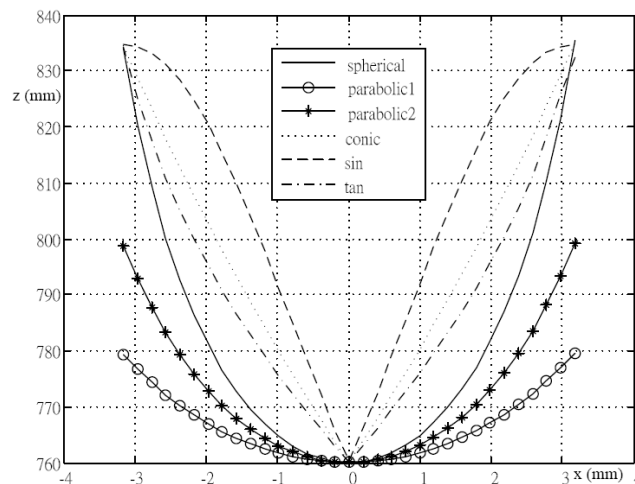


Fig. 3. The profiles of five distinct mirrors.

#### 4. A SIMULATOR OF OMNIDIRECTIONAL CAMERAS

In this section, a simulator is designed and implemented according to Eq. (11). The simulator also demonstrates the derived relationship. The simulator can compare the performance of these five mirror profiles mentioned as above. In addition, the simulator is utilized for analyzing the parameter variation of an omnidirectional camera in section

5. A calculation procedure summarizes the simulator implemented for omnidirectional cameras.

The simulator is implemented according to a perspective mirror model as shown in Fig. 2. The simulator colors the pixels of the image sensor with the color of the object surface position traced by the rays  $L_1$  and  $L_4$ . The main calculation makes use of the relationship between  $x_q$  and  $x_s$  as expressed by Eq. (11). The calculation of the simulator is summarized by the following procedure:

1. Take the calculated pixel position  $x_q$ ,
2. Get  $L_1$  from Eq. (3) according to focus  $\lambda$  and camera height  $H$ ,
3. Solve the intersection  $(x_r, z_r)$  between  $L_1$  and Eqs. (12)-(15) selected by regarding the mirror profiles,
4. Calculate the curvature of the mirror profile,  $z'(x_r)$ , at  $(x_r, z_r)$ ,
5. Calculate  $x_s$  from Eq. (11).

Exactly, the mirror surface of the omnidirectional camera is a three-dimensional space (*i.e.*  $x_r, y_r, z_r$ ). As above, the calculation procedure approximates it by two dimensions  $(x_r, z_r)$ . Besides, the variables of the image plane and the object surface are approximated by  $x_q$  and  $x_s$ , respectively. The approximation is according to Eq. (11), an easy understanding form. The practical calculation of the procedure regards  $x_q$  and  $x_s$  as the norm of a point in the polar coordinate. By the catadioptric principle, the polar angle of  $x_q$  equals to that of  $x_s$ . Hence, the beginning calculation only makes use of  $x_q$ , but reserves its polar angle. After solving  $x_s$ , the polar angle is accompanied to figure out an exact point on an object surface.

The simulator pastes the colors on the object surface on the pixels in the image sensor according to Eq. (11). During the calculation for pasting colors on the image plane, the central point of a pixel is regarded as  $x_q$  corresponded with  $x_s$  solved by the calculation procedure. After solving  $x_s$ , the object surface color on  $x_s$  is pasted on the pixel located at  $x_q$ .

The simulator also compares the performance of five mirror profiles installed in the omnidirectional camera. In the simulator, the parameters of the omnidirectional camera are  $L = 710\text{mm}$ ,  $H = 440\text{mm}$ ,  $R = 1,200\text{mm}$ , and  $\lambda = 3\text{mm}$ . Besides, the pixel dimension of the image sensor in the omnidirectional camera are  $640 \times 480$ , in which every pixel is square at length  $0.0099\text{mm}$ . Fig. 4 shows the pixel-distant curve, *i.e.* the relationship between  $x_q$  and  $x_s$ , conducted by the omnidirectional camera using the same size of spherical, parabolic, conical, tangent and sine mirror profiles, respectively. Notice that two parabolic mirrors which parameter  $f$  is  $0.6$  and  $0.8$ , respectively, are compared in the study. As shown in Fig. 6, the spherical mirror captures the largest scene, but the sine mirror captures the smallest one.

Fig. 5 shows the images captured by the omnidirectional camera. As shown in Fig. 5, the image of the colored square smoothly reduces area as it is far away from the camera center. The tangent, conical and sine mirrors get distorted images, but the scene taken by the tangent mirror is larger than by the conical and sine mirrors. However, the tangent, conical and sine mirrors lose some images around its center so that four colored squares placed on the image center are smaller than the others. This phenomenon can be verified

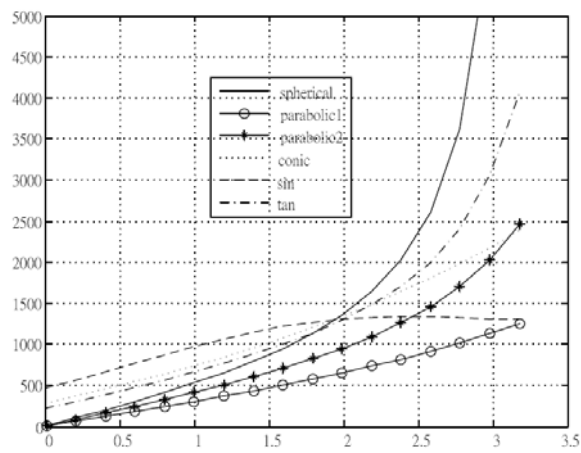


Fig. 4. The pixel-distant curves performed by five mirrors.

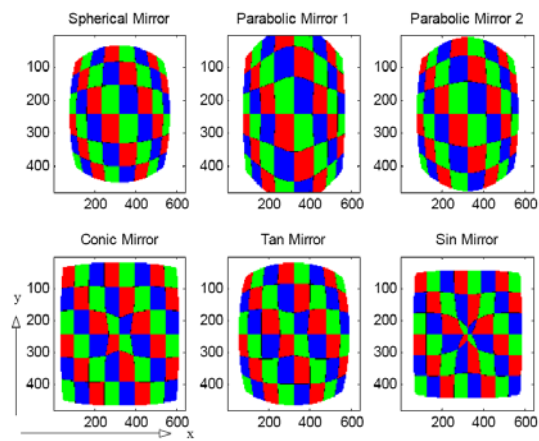


Fig. 5. The images captured by various mirrors.

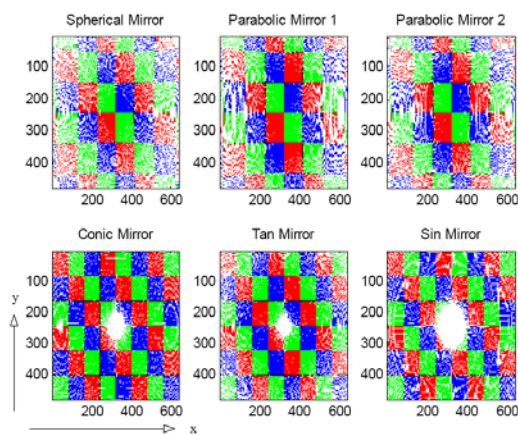


Fig. 6. The unwarped images by one point inside one pixel on the image sensor.

on Fig. 6 that the unwarped images of the tangent, conical, and sine mirrors have a small white circle in the center. The sizes of the small white circles are ordered by the tangent, conical, and sine mirrors. As a result, except the spherical mirror, the tangent mirror captures the largest scene, and has the smallest area lost as reading.

As shown in Fig. 6, the retrieved images result in lots of white spots. That is because the same size pixels in the image sensor capture unequal areas on the object surface. But here we let every pixel image be the same area on the object surface. So, some pieces of the object surface can not be retrieved, and miss its colors shown as the white spots. For eliminating the white spots, the algorithm of multiple calculation points inside one pixel is proposed. If one sensor pixel is separated by  $n$  points in vertical and horizontal edges, respectively, then this pixel makes use of  $n^2$  calculation points. The unwarped images retrieved by 16 calculation points inside one pixel are depicted in Fig. 7. Fig. 7 shows the algorithm with multiple calculation points captures very nice unwarped images.

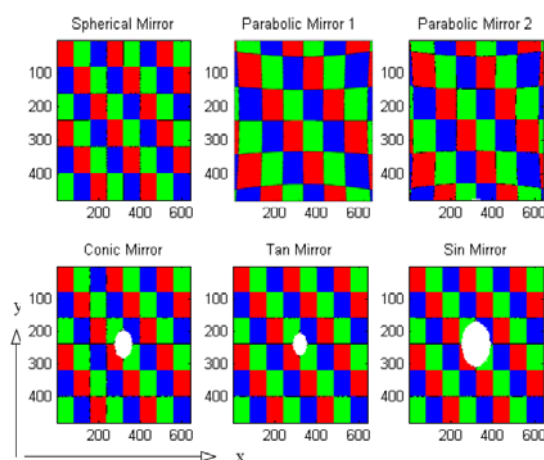


Fig. 7. The unwarped images by 16 points inside one pixel in an image sensor.

Notice that the algorithm of multiple calculation points used for the unwarped images exhaust much computation time. Let the object surface be divided into fixed size resolution that a user can accept. Then, the unwarped images solved from the object surface to the image plane maybe a good strategy for spending less computation time. However, the inverse function of Eq. (5) which is from the image plane to the object surface is needed for the strategy. It is difficult to solve the inverse of Eq. (5). To make a table based on Eq. (5) for the relationship between the object surface and the image plane is another strategy to solve the inverse relationship. To make the table is a good choice of solving the unwarped image for short computation time.

## 5. ANALYSIS OF IMAGE VARIATION DUE TO IMPRECISE PARAMETERS

In this section, the performance of the omnidirectional camera influenced by imprecise calibration is studied. The study is based on the relationship between  $x_s$  and  $x_q$  with

respect to the parameter variation. The influence focuses on comparing the performance of these five mirrors installed in the omnidirectional camera, respectively.

Installed with different mirror profiles, an omnidirectional camera has different relationships between  $x_q$  and  $x_s$ . Their relationships can be solved by the mirror surface equation and Eq. (11). Eqs. (12)-(16) are individually substituted into Eq. (11) as follows

$$x_s = (L + R - H - \sqrt{R^2 - x_{s1}^2}) \frac{x_q}{\lambda} + (L + R - \sqrt{R^2 - x_{s1}^2}) \frac{x_q (R^2 - 2x_{s1}^2) + 2\lambda x_{s1}}{\lambda(R^2 - 2x_{s1}^2) - 2x_q x_{s1}} \quad (17)$$

$$x_s = (L + R - H - \sqrt{R^2 - fx_{s1}^2}) \frac{x_q}{\lambda} + (L + R - \sqrt{R^2 - fx_{s1}^2}) \frac{x_q (R^2 - 2fx_{s1}^2) + 2\lambda fx_{s1}}{\lambda(R^2 - 2fx_{s1}^2) - 2x_q fx_{s1}} \quad (18)$$

$$x_s = \left(\frac{h}{w} x_{s1} + L - H\right) \frac{x_q}{\lambda} + \left(\frac{h}{w} x_{s1} + L\right) \frac{x_q \left(1 - \left(\frac{h}{w}\right)^2\right) + 2\lambda \frac{h}{w}}{\lambda \left(1 - \left(\frac{h}{w}\right)^2\right) - 2x_q \frac{h}{w}} \quad (19)$$

$$x_s = \left(h \tan\left(\frac{\pi}{4w} x_{s1}\right) + L - H\right) \frac{x_q}{\lambda} + \left(h \tan\left(\frac{\pi}{4w} x_{s1}\right) + L\right) \frac{\frac{x_q}{\lambda} + \frac{2z'(x_r)}{1 - z'(x_r)}}{1 - \frac{x_q}{\lambda} \frac{2z'(x_r)}{1 - z'(x_r)}} \quad (20)$$

$$\text{where } z'(x_{s1}) = \frac{h\pi}{4w} \sec^2\left(\frac{\pi}{4w} x_{s1}\right)$$

$$x_s = \left(h \sin\left(\frac{\pi}{2w} x_{s1}\right) + L - H\right) \frac{x_q}{\lambda} + \left(h \sin\left(\frac{\pi}{2w} x_{s1}\right) + L\right) \frac{\frac{x_q}{\lambda} + \frac{2z'(x_r)}{1 - z'(x_r)}}{1 - \frac{x_q}{\lambda} \frac{2z'(x_r)}{1 - z'(x_r)}} \quad (21)$$

$$\text{where } z'(x_{s1}) = \frac{h\pi}{2w} \cos\left(\frac{\pi}{2w} x_{s1}\right).$$

Eqs. (17)-(21) are the relationships as the omnidirectional camera consisted of spherical, conical, tangent and sine mirrors, respectively.

The various relationships with respect to the variation of mirror height  $L$  are said by the following Theory.

**Theory 1** Let the omnidirectional camera be regarded as a perspective mirror model as shown in Fig. 2. Then, the relationships between  $x_q$  and  $x_s$  obey Eqs. (17)-(21) as the omnidirectional camera installed by the mirrors of spherical, conical, tangent and sine profiles, respectively. The variation of these relationships with respect to camera height  $L$  is respectively said by

$$\frac{\partial x_s}{\partial L} = \frac{x_q}{\lambda} + \frac{x_q (R^2 - 2x_{s1}^2) + 2\lambda x_{s1}}{\lambda(R^2 - 2x_{s1}^2) - 2x_q x_{s1}}, \quad (22)$$

$$\frac{\partial x_s}{\partial L} = \frac{x_q}{\lambda} + \frac{x_q(R^2 - 2fx_{s1}^2) + 2\lambda fx_{s1}}{\lambda(R^2 - 2fx_{s1}^2) - 2x_q fx_{s1}}, \tag{23}$$

$$\frac{\partial x_s}{\partial L} = \frac{x_q}{\lambda} + \frac{x_q(1 - (\frac{h}{w})^2) + 2\lambda \frac{h}{w}}{\lambda(1 - (\frac{h}{w})^2) - 2x_q \frac{h}{w}}, \tag{24}$$

$$\frac{\partial x_s}{\partial L} = \frac{x_q}{\lambda} + \frac{\frac{x_q}{\lambda} + \frac{2z'(x_r)}{1 - z'(x_r)}}{1 - \frac{x_q}{\lambda} \frac{2z'(x_r)}{1 - z'(x_r)}}, \tag{25}$$

where  $z'(x_{s1}) = \frac{h\pi}{4w} \sec^2(\frac{\pi}{4w} x_{s1})$ ,

$$\frac{\partial x_s}{\partial L} = \frac{x_q}{\lambda} + \frac{\frac{x_q}{\lambda} + \frac{2z'(x_r)}{1 - z'(x_r)}}{1 - \frac{x_q}{\lambda} \frac{2z'(x_r)}{1 - z'(x_r)}}, \tag{26}$$

where  $z'(x_{s1}) = \frac{h\pi}{2w} \cos(\frac{\pi}{2w} x_{s1})$ .

**Proof:** As shown in Fig. 2,  $x_{s1} \ll x_s$ . So it is reasonable to neglect the variation of  $x_{s1}$  with respect to  $L$ . Therefore, the variation of  $x_s$  with respect to  $L$  can be approximated by the derivative of Eqs. (17)-(21) under considering  $x_{s1}$  as a constant. Then, it is trivial to obtain Eqs. (22)-(26) from the derivative of Eqs. (17)-(21) with respect to  $L$ .  $\square$

For practically comparing these five mirrors with same effective area, Eqs. (22)-(26) are figured out by data as shown in Fig. 8. Fig. 8 depicts  $\partial x_s/\partial L$  with respect to the

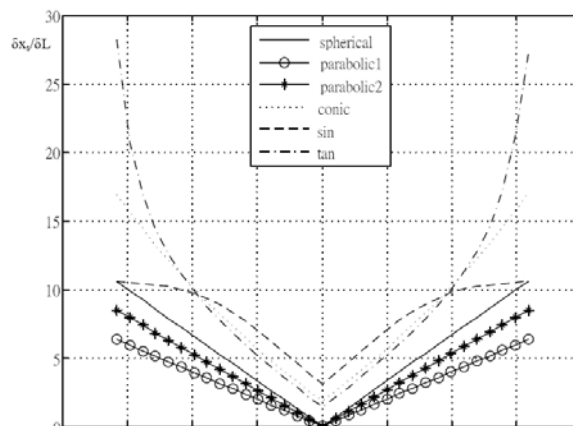


Fig. 8. The comparison of five-mirror variation ( $\partial x_s/\partial L$ ).

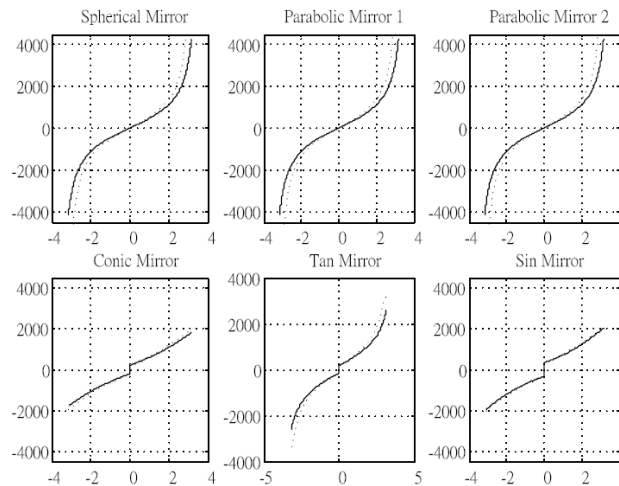


Fig. 9. The comparison of the pixel-distance curves as  $\Delta L = 50\text{mm}$  (Solid lines are original, but dot lines are variation).

variation of  $x_q$ . In Fig. 6, the spherical and conical mirrors have linear variation, the sine mirror has smooth variation, and the tangent mirror severely increases variation as the position moves away from the center of the image sensor. In addition, the relationships between  $x_q$  and  $x_s$  represented by the pixel-distance curves as shown in Fig. 6, influenced by parameter variation are compared in Fig. 9. Fig. 9 compares the variations of various mirror profiles as  $\Delta L = 50\text{mm}$ . As shown in Fig. 9, the sine mirror has the best performance as changing  $L$ .

It is easy to derive the influence of camera height variation (*i.e.*  $H$ ). The variation is the derivative of Eqs. (17)-(21) with respect to  $H$ . Then, the result is  $\frac{\partial x_s}{\partial H} - \frac{x_q}{\lambda}$  for all mirrors. As a result, all mirrors have the same image variation as missing precise camera height.

## 6. CONCLUSIONS AND DISCUSSIONS

In this paper, an omnidirectional camera installed by various mirror profiles was analyzed and compared. The relationship between the object surface and the image plane, concerned with mirror parameters was derived. The derived relationships including the omnidirectional camera consisted of the various mirror profiles benefit to show its performance influenced by parameter variations in equations. A simulator designed and implemented for the omnidirectional camera installed by spherical, parabolic, conical, tangent and sine mirrors, respectively, demonstrates the derived results. In addition, the simulator compares the performance of various mirrors influenced by imprecise calibration. In addition, the algorithm of multiple calculation points inside one pixel is proposed to resolve the problem that the white spots result from the object surface grabbed by the image sensor in different size. With the simulator, the algorithm retrieved the unwarped image very well as shown in Fig. 7.

The simulator compares the performance of the omnidirectional camera installed by the same size mirrors made of various profiles. There are five mirror profiles, spherical, parabolic, conical, tangent and sine, in the comparing study. The spherical mirror grabs the largest scene, and doesn't miss any image in a frame. And the features of parabolic mirrors are similar to the spherical mirror. The others, conical, tangent and sine mirrors miss a part of the image so that all of their unwarped images have a white circle, but the tangent mirror obtains the smallest white circle. *i.e.* The tangent mirror misses the least image. About the variation of missing precise sensor height, the distinct performance of five mirror profiles were compared by the designed simulator. The spherical mirror gets the linear variation, and its variation scale is smaller than the others. Although the sine mirror gets nonlinear variation, but the range of its variation is the narrowest. Therefore, after changing  $L$ , the image captured by the sine mirror is the most similar to before. In this paper, the comparison of various mirrors used in the omnidirectional camera is studied to provide how to choose mirrors for wide application, and to make the development of cheap omnidirectional cameras possible. The study of this paper paves a way to develop innovative kinds of omnidirectional camera in the future. In addition, an omnidirectional camera for 3D images is very useful for practical applications. However, in practical application, many other parameter variations such as horizontal variation also influence the performance of omnidirectional camera. It is also the further research on developing the innovative kinds of omnidirectional cameras.

## REFERENCES

1. Y. Yagi, "Omnidirectional sensing and its applications," *IEICE Transactions on Information and Systems*, Vol. E82-D, 1999, pp. 568-579.
2. T. Morita, Y. Yasukawa, Y. Inamoto, T. Uchiyama, and S. Kawakami, "Measurement in three dimensions by motion stereo and spherical mapping," in *Proceedings of IEEE Computer Vision and Pattern Recognition*, 1989, pp. 422-434.
3. Z. L. Cao, S. J. Oh, and E. L. Hall, "Dynamic omnidirectional vision for mobile robots," *Journal of Robotics Systems*, Vol. 3, 1986, pp. 5-17.
4. B. O. Matthews, D. Perdue, and E. L. Hall, "Omnidirectional vision applications for line following," in *Proceedings of SPIE Intelligent Robots and Computer Vision XIV: Algorithms, Techniques, Active Vision, and Materials Handling*, Vol. 2588, 1995, pp. 438-449.
5. P. Greguss, "The tube peeper: A new concept in endoscopy," *Optics and Laser Technology*, 1985, pp. 41-45.
6. P. Greguss, "PAL-optic based instruments for space research and robotics," *Laser and Optoelektronik*, Vol. 28, 1996, pp. 43-49.
7. Y. Yagi and S. Kawato, "Panorama scene analysis with conic projection," in *Proceedings of IEEE/RSJ International Workshop on Intelligent Robots and Systems*, 1990, pp. 181-187.
8. Y. Yagi, S. Kawato, and S. Tsuji, "Real-time omnidirectional image sensor (COPIS) for vision-guided navigation," *IEEE Transactions on Robotics and Automation*, Vol. 10, 1994, pp. 11-22.
9. J. Hong, X. Tan, B. Pinette, R. Weiss, and E. M. Riseman, "Image-based navigation

- using 360 views,” in *Proceedings of Image Understanding Workshop*, 1990, pp. 782-791.
10. S. L. Bogner, “An introduction to panospheric imaging,” in *Proceedings of IEEE International Conference on Systems, Man and Cybernetics*, Vol. 4, 1995, pp. 3099-3106.
  11. K. Yamazama, Y. Yagi, and M. Yachida, “Omnidirectional imaging with hyperbolic projection,” in *Proceedings of IEEE/RSJ International Conference on Intelligent Robots and Systems*, 1993, pp. 1029-1034.
  12. M. Yachida, “Omnidirectional sensing and combined multiple sensing,” in *Proceedings of IEEE and ATR Workshop on Computer Vision for Virtual Reality Based Human Communications*, 1998, pp. 20-27.
  13. V. Peri and S. K. Nayar, “Omnidirectional video system,” in *Proceedings of U.S.-Japan Graduate Student Forum in Robotics*, 1996, pp. 28-31.
  14. S. K. Nayar, “Catadioptric omnidirectional camera,” in *Proceedings of IEEE Conference Computer Vision and Pattern Recognition*, 1997, pp. 482-488.
  15. S. Baker and S. K. Nayar, “A theory of catadioptric image formation,” in *Proceedings of the 6th International Conference on Computer Vision*, 1998, pp. 35-42.
  16. S. Baker and S. K. Nayar, “A theory of single-viewpoint catadioptric image formation,” *International Journal of Computer Vision*, Vol. 35, 1999, pp. 175-196.
  17. R. A Hicks and R. Bajcsy, “Catadioptric sensors that approximate wide-angle perspective projections,” in *Proceedings of IEEE Conference on Computer Vision and Pattern Recognition*, 2000, pp. 1-7.
  18. P. Lima, A. Bonarini, C. Machado, F. Marchese, C. Marques, F. Ribeiro, and D. Sorrenti, “Omni-directional catadioptric vision for soccer robots,” *Robotics and Autonomous Systems*, Vol. 36, 2001, pp. 87-102.

**Kuo-Yang Tu (杜國洋)** was born in Tainan, Taiwan, R.O.C., in 1961. He received the B.S., M.S. and Ph.D. degrees in Electrical Engineering from National Taiwan University of Science and Technology, Taipei, Taiwan, in 1987, 1992 and 1998, respectively. In 1998, he was appointed as Associate Professor with the Department of Electronic Engineering, Hwa-Hsia College of Technology and Commerce. Currently, he is an Associate Professor with the Institute of Systems and Control Engineering, National Kaohsiung First University of Science and Technology. Since 1999, he is a patent screening member of the National Intellectual Property Office, Ministry of Economic Affairs, Taipei, Taiwan, R.O.C. His current research interests and publications are in the area of intelligent computation, multi-agent system, system integration and robotics. Specially, he had organized a team of robotics soccer for the competition of small-size league in EuRoboCup99 and RoboCup00 held on Amsterdam and Seattle, respectively. Dr. Tu is a member of the IEEE Systems, Man, and Cybernetics Society, the IEEE Control Systems Society, the IEEE Computer Society, and the IEEE Robotics and Automation Society.